

QUASI-STEADY AERODYNAMIC ANALYSIS OF PROPELLER–WING INTERACTION

JINSOO CHO* AND JAEHEON CHO

Department of Mechanical Engineering, Hanyang University, Seoul 133-791, South Korea

SUMMARY

A quasi-steady scheme for the analysis of aerodynamic interaction between a propeller and a wing has been developed. The quasi-steady analysis uses a 3D steady vortex lattice method for the propeller and a 3D unsteady panel method for the wing. The aerodynamic coupling is represented by periodic loads, which are decomposed into harmonics and the harmonic amplitudes are found iteratively. Each stage of the iteration involves the solution of an isolated propeller or wing problem, the interaction being done through the Fourier transform of the induced velocity field. The propeller analysis code was validated by comparing the predicted velocity field about an isolated propeller with detailed laser Doppler velocimeter measurements, and the quasi-steady scheme by comparison with mean loads measured in a wing–propeller experiment. Comparisons have also been made among the fluctuating loads predicted by the present method, an unsteady panel scheme and a quasi-steady vortex lattice scheme. Copyright © 1999 John Wiley & Sons, Ltd.

KEY WORDS: aerodynamics; propeller–wing interaction; quasi-steady analysis

1. INTRODUCTION

It has been reported that lift augmentation and drag reduction on a wing can result from propeller–wing interaction. As will be shown later, a number of attempts have been made to solve the problems arising from the interaction of the wing–propeller system. Various quasi-steady and unsteady methods were applied to compute the unsteady loads resulting from the interaction. These unsteady loads must be evaluated for the aeroelastic analysis of an interacting system. It is the objective of this study to present an efficient numerical method for the prediction of the unsteady aerodynamic forces that arise from the interaction.

Several studies have been made of the effects of the propeller slipstream on wing performance, using a variety of slipstream models. Kleinstein and Liu [1] treated the slipstream as a simple circular jet. Loth and Loth [2] added rigid rotation. Miranda and Brennan [3] used a more realistic vortex tube model of the slipstream. In all three studies, the propwash field was prescribed and the wing performance was obtained from the lifting line theory. In contrast, Kroo [4] examined the optimization of integrated performance using a relatively simple model of the interference between rotor and wing.

Unsteady loads have been calculated by Rangwalla and Wilson [5] using a time marched incompressible panel method with a free wake model. Lee [6] used a quasi-steady vortex lattice

* Correspondence to: Department of Mechanical Engineering, Hanyang University, Seoul 133-791, South Korea.

method for wing–propeller interference. This scheme does predict the unsteady loads, but the neglect of spanwise vortex shedding, which is implicit in the quasi-steady approximation, casts some doubt on the accuracy of the predicted fluctuations, particularly for the highly reduced frequencies presented on the wing. Recently, Cho and Williams [7] used a lifting surface panel method in the frequency domain for wing–propeller interference. This scheme was developed by Williams [8,9] for the aerodynamic and aeroelastic analysis of single rotation propellers. In that application, the blade loading is represented by a single frequency. The extension to wing–propeller interference requires that loads be represented with multiple harmonics, which interact through the induced velocity field.

The induced velocity field calculation has been validated by comparison with laser Doppler velocimeter (LDV) measurements taken by Sundar [10] around a single rotation propeller. Similar LDV data, for a different rotor, were reported by Lepicovski and Bell [11]. Iterative velocity field calculations for Sundar’s configuration based on a Euler code and vortex lattice model have been done by Usab *et al.* [12].

The present wing–propeller interference calculation has been validated by comparisons with wind tunnel measurements made by Witkowski [13], with Lee’s quasi-steady vortex lattice analysis [6] and with Cho and Williams’ unsteady panel analysis [7] of the same configuration.

2. METHODOLOGY

2.1. Propeller

A vortex lattice method (VLM) is used to model the propellers. A vortex line is the solution of the Laplace equation, which is a governing equation of incompressible, inviscid and potential flow, and the flow tangency boundary condition is used.

$$\nabla^2\Phi(x, y, z) = 0 : \text{governing equation}, \quad (1)$$

$$\nabla(\Phi + \Phi_0) \cdot \vec{n} = 0 : \text{boundary equation}, \quad (2)$$

where Φ is the velocity potential that is produced by a singularity element, Φ_0 is the velocity potential of free stream and \vec{n} is the normal unit vector on the blade surface. The horseshoe vortices used are composed of bound vortices on the 1/4 chord line, which represent the lifting component and trailing vortices that represent the wake. Trailing vortex, helical vortex lines must continue infinitely in the flow in order not to violate Helmholtz’s law. Induced velocity caused by a vortex line can be calculated by the Biot–Savart law. In order to make the normal velocity component (which is induced at each control point by every lifting line) satisfy boundary condition, the following linear equation is used:

$$V_{Rj} = \sum_i \frac{\Gamma_j}{4\pi} F_{ij}, \quad (3)$$

(normal velocity induced at the j th control point by vortices) where F represents the aerodynamic force that can be obtained by the integration of pressure difference. Using Equation (3) the following matrix equation can be set up:

$$A_{RR} \cdot \Gamma = V_R. \quad (4)$$

Then A_{RR} is the known aerodynamic influence coefficient (AIC) matrix between the rotor lattices, and V_R is the upwash of the rotor, which is the boundary condition.

Using calculated vortex strength Γ , the aerodynamic forces on the propeller can be calculated using the Kutta–Joukowski law, and the AIC matrix between the rotor (propeller) and the wing, A_{WR} , will be determined by using the Biot–Savart law. The pressure difference of a horseshoe vortex element on the j th radial position can be represented as follows:

$$\Delta p_{r_j} = \rho \sqrt{(r_j \Omega)^2 + V_\infty^2} \frac{\Delta \Gamma_j}{\Delta r_j}. \tag{5}$$

The application of the VLM to model the propellers, as described above, has been given by several authors [14–17]. The detailed equation used for the present VLM for propellers can be found easily in [16–18]. The compressibility effect on the propeller can be accounted for by using the Prandtl–Glauert rule.

2.2. Wing

A non-planar lifting surface method used for analysis of the wing is based on the linear compressible lifting surface theory. To explain briefly the method used, consider linearized compressible flow in which the initial disturbances vanish from the lifting surfaces. Induced velocity at an arbitrary point \vec{x} can be solved by the momentum equation, small disturbance theory and the boundary condition of lifting surface with the assumption that flow is inviscid, irrotational and isentropic. A point on lifting surface \vec{x}_0 with unit normal \vec{n}_0 is assigned a transformed pressure differential $\Delta p = \rho U_0 P$ acting in the direction $+\vec{n}_0$. The lifting surface induces a transformed velocity \vec{U}_W at an arbitrary point \vec{x} , which is given by an integral over the lifting surface.

$$\vec{U}_W(\vec{x}) = \iint P_W(\vec{x}_0) \vec{K}_W(\vec{x}, \vec{x}_0) dA_0, \tag{6}$$

where \vec{K}_W is the kernel function of the planar wing. The integral can be discretized by assuming a piecewise constant load on each wing panel,

$$A_{WW} \cdot P_W = V_W. \tag{7}$$

A_{WW} is the aerodynamic influence coefficient matrix between the wing panels, and V_W is the upwash of the wing. Then, A_{WW} is expressed as follows:

$$A_{WW} = \iint_{\text{wing}} K_W(x_W - x_0, y_W - y_0) dx_0 dy_0, \tag{8}$$

where x_W and y_W denote arbitrary control point positions on the wing.

The AIC matrix between the wing and the propeller, A_{RW} , can be expressed as follows, when the non-planar kernel, $K_{W_{\text{non-planar}}}$, is used:

$$A_{RW} = \iint_{\text{wing}} K_{W_{\text{non-planar}}}(x_R - x_0, y_R - y_0, z_R) dx_0 dy_0, \tag{9}$$

where x_R, y_R, z_R are arbitrary field points on the rotor plane. The explicit expressions of K for both planar and non-planar cases will be found in References [19,20].

2.3. Wing–propeller interaction

The quasi-steady interaction between a wing and rotor can be expressed by a pair of linear relations between the instantaneous normal velocity (V) and the pressure difference (Δp) on the respective lifting surfaces.

$$\begin{aligned} V_R &= A_{RR} \cdot \Delta p_R + A_{RW} \cdot \Delta p_W, \\ V_W &= A_{WR} \cdot \Delta p_R + A_{WW} \cdot \Delta p_W. \end{aligned} \tag{10}$$

The coefficients of A are linear integral space–time operators, as explained already. The solution (for Δp) can clearly be decomposed into the sum of rotor-driven ($V_W = 0$) parts. It is assumed that the wing and rotor are rigid and the rotor is at zero incidence.

The load on the j th blade, Δp_{R_j} can be represented as the function of vortex strength Γ_j that varies with radius (Equation (5)). The wing load, Δp_W , can be expanded in harmonics by the periodicity of the interaction

$$\Delta p_W = \sum_n P_{W_n} e^{inN\Omega t}, \tag{11}$$

where V_∞ is the free stream velocity, Ω the angular velocity of rotor, N the number of rotor blades, n the harmonic index.

The objective is to compute the vortex strength Γ and the harmonic load coefficient P_{W_n} for given normal velocities V . By substituting Equations (5) and (11) into Equation (10) and separating the harmonics, we get

$$\begin{aligned} \bar{A}_{RR} \cdot \Gamma &= \bar{V}_R, \\ \bar{A}_{WW}(nN\Omega) \cdot P_{W_n} &= \bar{V}_{W_n}, \end{aligned} \tag{12}$$

where \bar{A}_{RR} denotes the reference blade operator and $\bar{A}_{WW}(\omega)$ denotes the wing operator for simple harmonic motion with frequency ω . \bar{V}_R is the normal velocity on the blade surface modified by the induced velocity from the wing. \bar{V}_{W_n} is the complex harmonic amplitudes of the normal velocity on the wing surface modified by the induced velocity from the blade. Given \bar{V} , Equation (12) represents separate problems for the rotor and wing. Of course, the \bar{V} values are not given, but depend, in a complicated way, on the loads. The induced velocity field by the rotor is obtained by the Biot–Savart law. This velocity field, being of the period $\Delta\theta = 2\pi/N$ by the rotation of the rotor, can be Fourier-expanded in the rotor frame, $\bar{\theta}$, with frequency Ω .

$$\vec{u}_R(\bar{\theta}) = \sum_{k=-\infty}^{\infty} \vec{U}_{R_k}(k\Omega) e^{ik\bar{\theta}}, \tag{13}$$

where

$$\vec{U}_{R_k} = \frac{1}{\Delta\theta} \int_0^{\Delta\theta} \vec{u}_R(\bar{\theta}) e^{-ik\bar{\theta}} d\bar{\theta}, \quad k = 0, \pm 1, \dots \tag{14}$$

$$\vec{U}_{R_{-k}} = \text{complex conjugate of } \vec{U}_{R_k}.$$

The velocity field of Equation (13) in $\bar{\theta}$ is transformed to the wing frame ($\theta = \bar{\theta} - \Omega t$, Figure 2).

$$\vec{u}_R(\theta, t) = \sum_k [\vec{U}_{R_k} e^{ik\theta}] e^{ik\Omega t}. \tag{15}$$

The velocity field $\vec{U}_{R_k} e^{ik\theta}$ corresponds to the wing frame frequency $k\Omega$ and therefore contributes, to the wing normal velocity \bar{V}_{W_k} in Equation (12), an amount

$$\Delta \bar{V}_{W_k} = -\vec{n}_W \cdot \vec{U}_{R_k} e^{ik\theta}, \tag{16}$$

where \vec{n}_W is the normal to the wing camber surface.

Similarly, each harmonic P_{W_n} on the wing produces a velocity field that is a simple harmonic in the frame,

$$\vec{u}_{W_n} = \vec{U}_{W_n}(\theta) e^{inN\Omega t}, \tag{17}$$

where the complex amplitude is found by an integral over the wing,

$$\vec{U}_{W_n} = \iint P_{W_n}(\vec{x}_0) \vec{K}_W(\vec{x}, \vec{x}_0) dA_0. \tag{18}$$

Note that the wing operator \bar{A}_{WW} is a normal projection of Equation (18) on the wing. This velocity field too can be Fourier-expanded in θ and transferred to the rotor frame,

$$\vec{u}_{W_n} = \sum_k [\vec{U}_{W_{nk}} e^{ik\bar{\theta}}] e^{i(nN-k)\Omega t}, \tag{19}$$

where

$$\vec{U}_{W_{nk}} = \frac{1}{2\pi} \int_0^{2\pi} \vec{U}_{W_n}(\theta) e^{-ik\bar{\theta}} d\theta. \tag{20}$$

The velocity field $\vec{U}_{W_{nk}} e^{-ik\bar{\theta}}$ corresponds to the rotor frame frequency $(nN-k)\Omega$. But due to steady state analysis of the rotor, only the mean value (0th frequency, $k=0$) in Equations (19) and (20) contributes, to the rotor normal velocity \bar{V}_R in Equation (12), an amount,

$$\Delta \bar{V}_R = -\vec{n}_R \cdot \vec{U}_{W_{n0}}, \tag{21}$$

where

$$\vec{U}_{W_{n0}} = \frac{1}{2\pi} \int_0^{2\pi} \vec{U}_{W_n}(\theta) d\theta$$

and \vec{n}_R are normal to the reference blade.

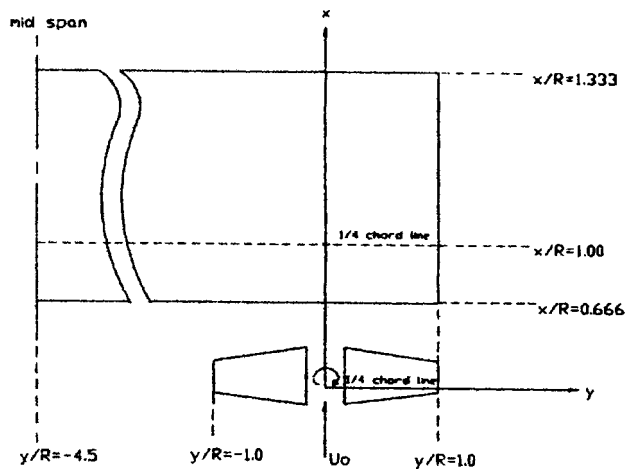


Figure 1. Propeller-wing configuration.

2.4. Iterative scheme

The calculation is performed iteratively in the following sequence.

For each rotor harmonic:

- (1) Compute prop loads.
- (2) Compute propwash field around wing.
- (3) Fourier decompose propwash.
- (4) Distribute Fourier component to wing normal velocity harmonics.

For each wing harmonic:

- (5) Compute wing loads.
- (6) Compute wingwash field around prop.
- (7) Fourier decompose wingwash.
- (8) Distribute only 0th harmonic Fourier component to prop normal velocity harmonics.

This sequence is repeated to convergence. On initial entry, which could be either step (1) or (5), the interaction is ignored, and only one harmonic load is computed.

At the discrete level, the solution of Equation (12) involves the inversion of a large system of simultaneous linear equations. To avoid repetitive calculation, the inverse influence coefficient matrix for each harmonic can be computed once and stored. The load calculation in steps (1) and (5) of the iteration is then reduced to a matrix–vector multiplication.

3. RESULTS

Most of the results reported here were obtained using seven chordwise panels on both the wing and rotor. Roughly 12–15 radial rows were used on the rotor blade and about 30 spanwise on the wing (concentrated in the disk plane). These numbers are adequate to resolve the integrated loads to within a few percent [7].

3.1. Isolated propeller velocity field

To validate the present 3D VLM formulation, the velocity calculation was tested on an isolated propeller, for which Sundar [10] has made detailed LDV measurements. The propeller has two blades, whose tip radius is 6 in. The blades have a straight, constant chord and have an aspect ratio of 3 with a fixed pitch of 45.4° at $3/4$ blade tip radius, an NACA 0010 airfoil sections and a helical twist distribution.

Figure 3 shows the predicted circumferentially averaged velocities, excluding blade thickness and centerbody, using the present 3D vortex lattice formulation. It can be seen in the figure that the axial velocity components are bigger than free stream velocity (i.e. $U_x/U_0 > 1$), and the radial velocity components are negative (i.e. $U_r/U_0 < 0$), which shows that the expected axial acceleration balanced by a radial inflow. The mean swirl is zero upstream and constant downstream from the rotor. The circumferential variation of velocity at one station is shown in Figure 4. In the figure caption, $x/R = 0.267$ and $r/R = 0.933$ imply that the LDV probe is located axially, slightly apart downstream from the trailing edge of the blade root and radially inboard near the tip. The present result is compared with the measured data to validate the present 3D vortex lattice formulation for the propeller. It can be easily seen for the figure that the present VLM calculation shows good agreement with measured data in axial velocity components, and a small amount of constant offset in tangential and radial velocity

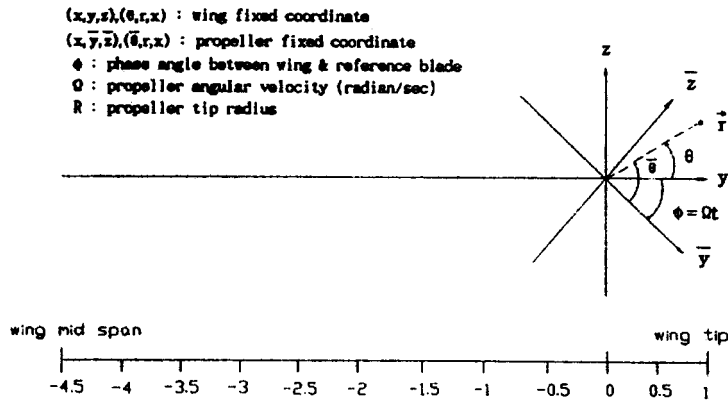


Figure 2. Co-ordinate system.

components (note different ordinate scales for the three velocity components in the figure). Although the calculated tangential and radial velocity show the same azimuthal variation with measured data, the fixed helical wake model used in the present method produced a constant amount offset and small phase shift. It can be concluded from this result that the blade loading for the case considered here is well-predicted using the present VLM.

Figure 5 gives the harmonic decomposition of the tangential velocities at a downstream station of $x/R = 1.00$ as a function of the spanwise location. In the figure, the non-zero (8°) angle of attack of the wing produces the asymmetry of the curves about $y/R = 0.0$. This result corresponds to the first-order wing upwash at the quarter chord in the wing-propeller calculation discussed in the next section. Note that the amplitudes decrease rapidly with increasing frequency ($n = 5$ corresponds to a 10Ω wing excitation). Based on this result, the wing-propeller interaction was truncated at the fifth harmonic.

3.2. Propeller-wing interaction

Results will be presented for the propeller-wing configuration shown in Figure 1, which is the same as Cho's [7]. The propeller is identical to the rotor examined in the last section. The wing is rectangular, $AR = 8.25$ (chord length = 8 in., wing span = 66 in.), with NACA 0010 section. The wing and rotor are separately articulated and mounted so that the axis of rotation lies in the wing symmetry plane (at $\alpha = 8^\circ$). The free stream Mach number is 0.1 and the two advance ratios of $J = 1.1$ and $J = 1.66$ considered here correspond to the blade tip Mach numbers of 0.29 and 0.21 (blade root Mach numbers of 0.13 and 0.12) respectively, where the compressibility effect is almost negligible.

Wing and blade thickness are ignored in the calculations because of the relatively large separation between the two. The system is assumed to be symmetric about the wing mid-span. In contrast, the experiment used a wall mounted semi-span model, and Lee [6] used a full span wing with a single tip mounted rotor in this quasi-steady vortex lattice simulation.

We will first examine some properties of the mean loading, for which there are experimental data. The characteristic features of the unsteady fluctuations will then be described, with comparisons with Lee's [6] quasi-steady analysis and Cho's [7] unsteady analysis. Cho's unsteady results are based on 3D unsteady lifting surface formulation for both propeller and wing, and Lee's quasi-steady results use steady VLM for both propeller and wing, whereas the present method models the propeller with vortex lattice and the wing with 3D unsteady panels, as explained in Section 2.

Figure 6 shows the effect of the propeller on the mean sectional lift distribution on the wing half span for a case where $\alpha = 8^\circ$ and $J = 1.66$. Three results are shown. The curve labeled 'Wing Only' is the predicted load without a propeller. The curve labeled '0th Propwash' is the result of simply imposing the isolated propeller wake swirl on the wing without accounting for the back influence of the wing on the rotor. Finally, the curve labeled 'Full Interaction' shows the mean loading i th complete interaction. Note that the prop effect of complete interaction is to slightly decrease the loads below the level set by the '0th Propwash' case, but the change is very small. A similar comparison for the propeller is shown in Figure 7. There is practically no change in the main thrust loading due to the interaction.

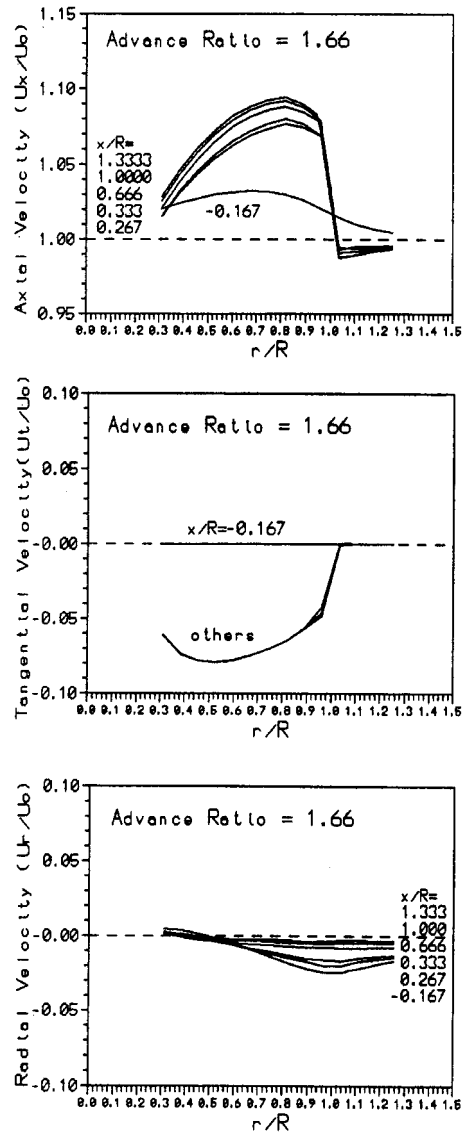


Figure 3. Predicted averaged axial, tangential and radial velocity.

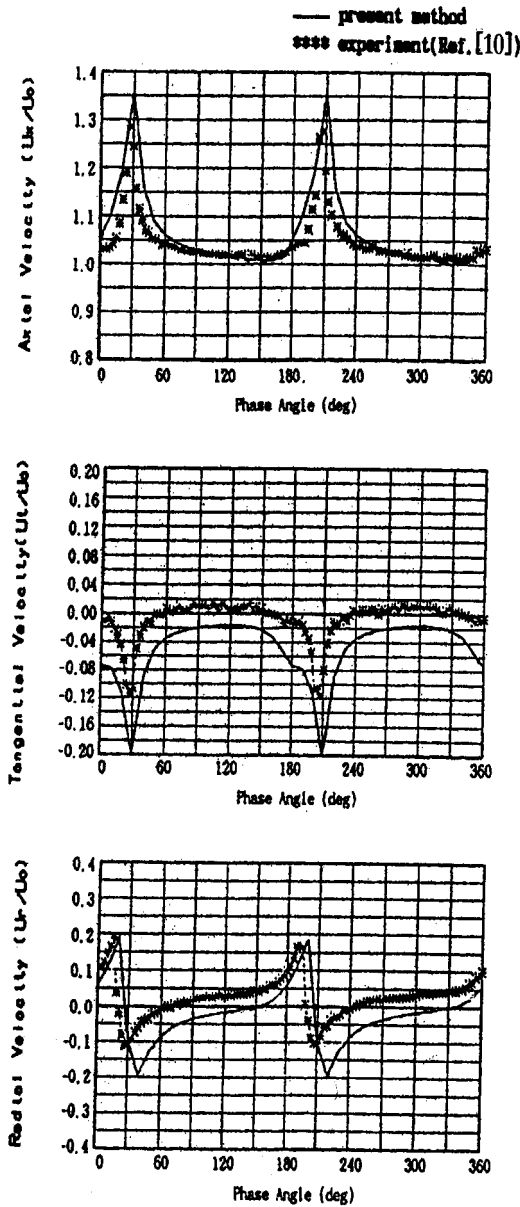


Figure 4. Downstream velocity profiles ($x/R = 0.267$, $r/R = 0.933$, $J = 1.66$).

The total (time-averaged) lift and drag on the wing as a function of the angle of attack are shown in Figures 8 and 9 respectively. Results of the present method, the unsteady method (Cho), the quasi-steady method (Lee), and the experiment are shown. The calculations agree remarkably well with the experiment, apart from the expected roll-off of the measured values at the high angle of attack (the wing stalls around $\alpha = 14^\circ$). The drag includes a viscous component (whose magnitude is estimated from sectional data in Reference [21]) as well as induced drag, which is indicated by the dotted line in Figure 9. Note that the induced drag is

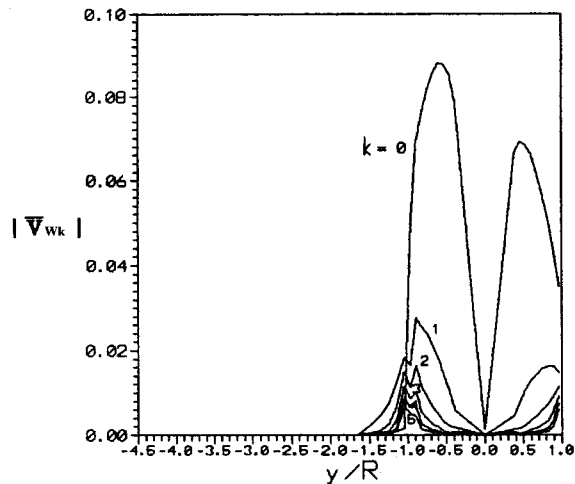


Figure 5. Fourier transformed upwash distribution ($J = 1.66$, $\alpha = 8^\circ$, $x/R = 1.00$).

slightly negative at low incidence, reflecting the fact that the prop swirl actually induces thrust on the wing.

At the advance ratio $J = 1.66$, the corresponding reduced frequency k on the wing (based on the fundamental frequency of 2Ω , wing chord, and free stream velocity) is 5.05, and the local reduced frequency k on the prop (based on Ω , prop chord and relative velocity) is 0.36.

As mentioned in Section 1, lift augmentation and drag reduction result from the propeller–wing interaction. This drag reduction is shown in Figure 10. ΔC_D is the difference between C_D of the interacting system and wing performance alone for the same value of C_L . The present method shows a large value with comparisons with the unsteady, the quasi-steady calculation and the experiment. It is considered that this is due to the difference in Figure 9. Figure 11 shows the time history of the wing sectional lift coefficient after a propeller–wing interaction.

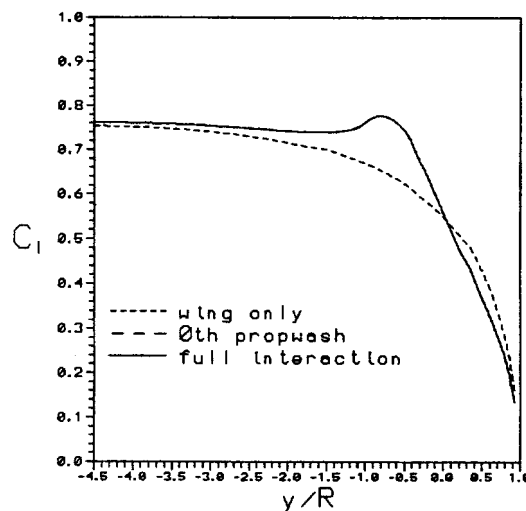


Figure 6. Mean sectional lift coefficient ($J = 1.66$, $\alpha = 8^\circ$).

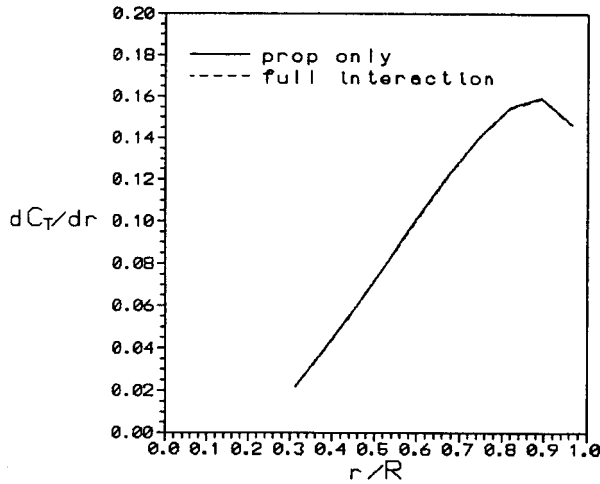


Figure 7. Mean sectional thrust on the propeller ($J = 1.66$, $\alpha = 8^\circ$).

Note that C_L is largest at around $\phi = 30^\circ$, when the propeller wake hits around the quarter chord of wing.

Figure 12 shows the time history of total lift on the wing for the heavily loaded prop case at $J = 1.10$ with comparisons with Cho's [7] unsteady analysis and Lee's [6] quasi-steady analysis. It can be easily seen in the figure that the present method is close to Cho's 0th propwash unsteady result, whereas Lee's quasi-steady results deviates from the unsteady result not only in magnitude but also in phase. This proves that Lee's quasi-steady method is unable to predict the fluctuating wing loads at the highly reduced frequency k on the wing (based on the fundamental frequency of 2Ω , wing chord, and free stream velocity) of 7.61, which was pointed out already in the Section 1. Figure 13 shows the contributions of harmonics to the present result in Figure 12. It can be concluded from Figures 12 and 13 that the higher harmonics have a negligible effect on the present quasi-steady solution in contrast to the Cho's

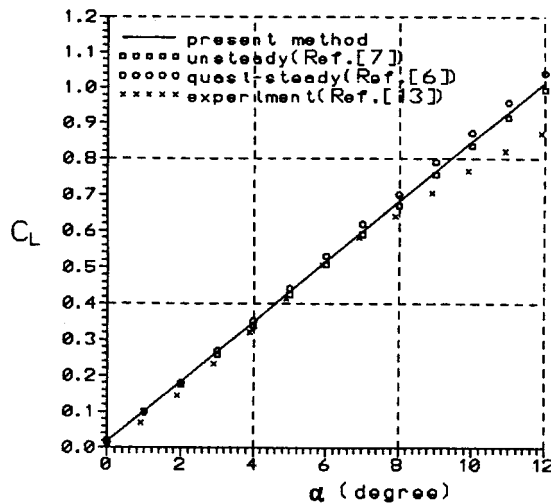


Figure 8. Mean total lift coefficient.

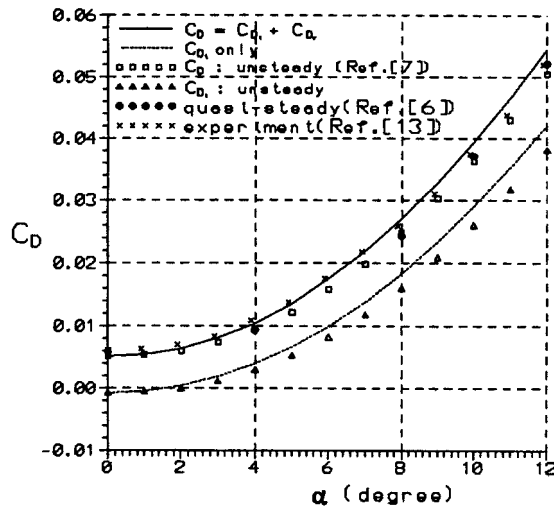


Figure 9. Mean total drag coefficient.

unsteady solution. In contrast to the result of Figure 12, the sectional thrust on the propeller at 3/4 blade tip radius for the same advance ratio of $J = 1.10$, shown in Figure 14, shows clearly that the unsteady effects are not important here since the present, the Lee's quasi-steady and the unsteady analysis give basically the same time histories (the mean value offset between the three is the discretization error coming from the prop-only results). This is understandable since the local reduced frequency k on the prop (based on Ω , prop chord and relative velocity) is only 0.40 for the case.

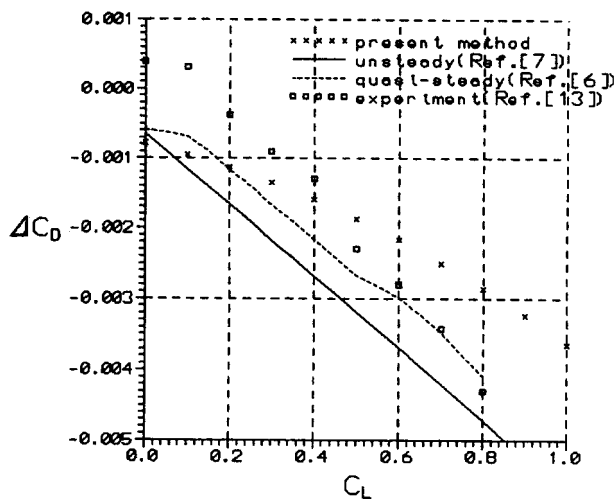


Figure 10. Drag reduction vs. lift due to interaction.

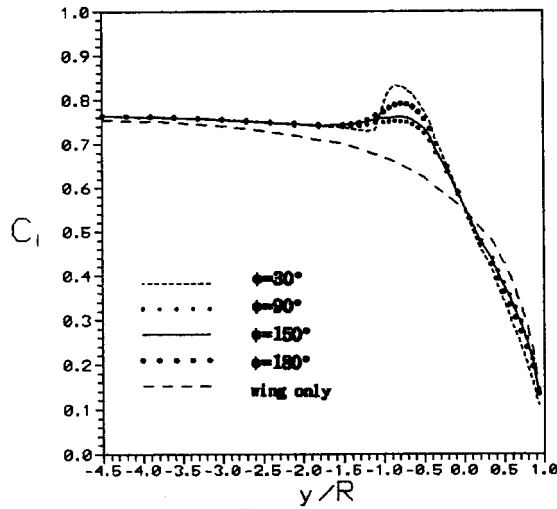


Figure 11. Time history of sectional lift coefficient ($J = 1.66, \alpha = 8^\circ$).

Note that, in the absence of comparable unsteady measured data, the unsteady panel method used for the wing can give poor results at extremely high frequencies. This may become a serious problem when the propeller advance ratio decreases (higher rpm) and when the number of blades increases (high blade passing frequency).

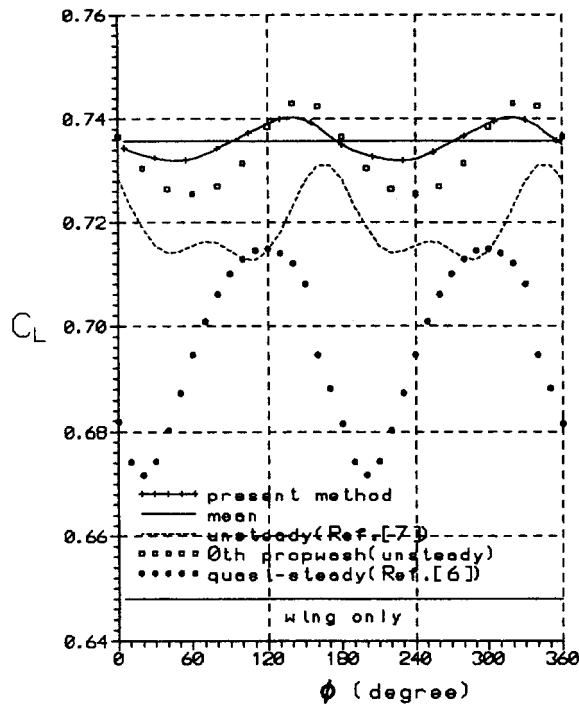


Figure 12. Time history of wing lift ($J = 1.66, \alpha = 8^\circ$).

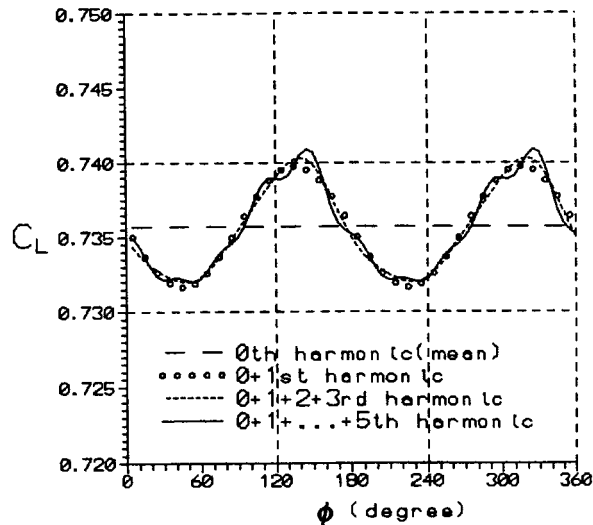


Figure 13. Contributions of harmonics to lift time history ($J = 1.10$, $\alpha = 8^\circ$).

4. CONCLUSIONS

The lifting line method used here has been shown to predict a good agreement with measured velocity field data for a single rotation propeller and a generally good agreement with measured loads on a wing-propeller system. The unsteady load predictions relatively agree with Lee's quasi-steady analysis and Cho and Williams' unsteady analysis on the rotor, where the reduced frequencies are relatively low, but disagree on the wing, where the reduced frequencies are high. But the present method is closer to unsteady analysis than to Lee's quasi-steady analysis.

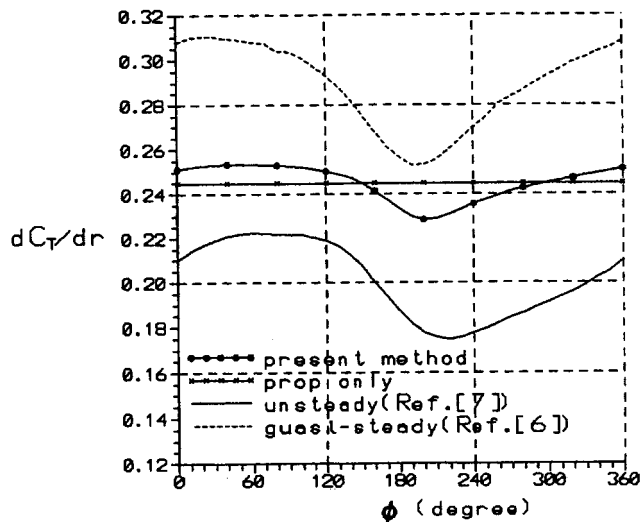


Figure 14. Time history of blade sectional thrust ($r/R = 0.75$, $J = 1.10$, $\alpha = 8^\circ$).

The results of the propeller–wing interaction analysis indicate that useful performance predictions can be made with a simplified model, wherein the circumferentially averaged (isolated) propwash is imposed on the wing to get the modified steady wing loading, and circumferentially averaged (isolated) wingwash is imposed on the prop to get the modified steady blade loading. All other interaction terms appear to have only a small effect on the mean performance.

It was also found that for the cases examined using the present quasi-steady analysis method, good estimates of the load fluctuations were obtained with just the first few harmonics. However, care should be taken dealing with extremely high frequency problems. What is required is a better numerical scheme for evaluating high frequency response. Much more importantly, what is required is the experimental data at high frequencies with which to compare.

APPENDIX A. NOMENCLATURE

A	linear integral time–space operator (aerodynamic influence coefficient)
\bar{A}	complex harmonic operator
AR	aspect ratio
C_D	drag coefficient
C_L	lift coefficient
F	aerodynamic forces
J	advance ratio
k	reduced frequency based on chord
K	kernel function of wing
m	total number of rotor lattices
n	harmonic index
\hat{n}	unit normal vector on the blade surface
N	number of rotor blade
Δp	pressure difference
P	harmonic load coefficient
R	rotor radius
r, θ, z	cylindrical co-ordinate system
\vec{u}	induced velocity
\vec{U}	transformed velocity
V	upwash (instantaneous normal velocity)
\bar{V}	complex harmonic amplitude of the normal velocity
x, y, z	Cartesian co-ordinate system

Greek letters

α	angle of attack
ϕ	phase angle between the reference propeller blade and the wing
ρ	density
ω	frequency of simple harmonic motion
Γ	vortex strength
Φ	velocity potential
Ω	angular velocity of rotor

Subscripts

R	rotor
W	wing
o	free stream condition

REFERENCES

1. G. Kleinstein and C.H. Liu, 'Application of airfoil theory for non-uniform streams to wing-propeller interaction', *J. Aircraft*, **9**, 137–142 (1972).
2. J.L. Loth and F. Loth, 'Induced drag reduction with wing tip mounted propellers', *AIAA Paper 84-2149*, 1984.
3. L.R. Miranda and J.E. Brennan, 'Aerodynamic effects of wingtipmounted propellers and turbines', *AIAA Paper 86-1802*, 1986.
4. I. Kroo, 'Propeller-wing integration for minimum induced loss', *J. Aircraft*, **23**, 561–565 (1986).
5. A.A. Rangwalla and L.N. Wilson, 'Application of panel code to unsteady wing-propeller interference', *J. Aircraft*, **24**, 568–571 (1987).
6. K.H. Lee, 'A computational investigation of propeller-wing interactions', *Ms. Thesis*, Department of Aeronautics and Astronautics, Purdue University, 1988.
7. J. Cho and M.H. Williams, 'Propeller-wing interaction using a frequency domain panel method', *J. Aircraft*, **27**, 196–203 (1990).
8. M.H. Williams, 'An unsteady lifting surface theory for single rotation propellers', *Purdue University Report*, 1985.
9. M.H. Williams and C. Hwang, 'Three-dimensional unsteady aerodynamics and aeroelastic response of advanced turboprops', *AIAA Paper 86-0846*, 1986.
10. R.M. Sundar, 'An experimental investigation of propeller wakes using a laser Doppler velocimeter', *Ph.D. Thesis*, Department of Aeronautics and Astronautics, Purdue University, 1985.
11. J. Lepicovsky and W.A. Bell, 'Aerodynamic measurements about a rotating propeller with a laser velocimeter', *J. Aircraft*, **21**, 264–271 (1984).
12. W.J. Usab, K.H. Lee and J.P. Sullivan, 'A comparison of numerical simulation and experimental measurements of flow through propellers', *AIAA Paper 88-367*, 1988.
13. D.P. Witkowski, 'Experimental investigation of propeller-wing interactions', *Ms. Thesis*, Department of Aeronautics and Astronautics, Purdue University, 1988.
14. V.E. Baskin, L.S. Vil'dgrube, Ye.S. Vozhdayev and G.I. Mayhapan, 'The theory of the lifting airscrew', *NASA TT F-823*, 1976.
15. J.E. Kerwin and R. Leopard, 'A design theory for subcavitating propellers', *Trans. Soc. Naval Arch. Marine Eng.*, **72**, 214–219 (1964).
16. J.P. Sullivan, 'The effect of blade sweep on performance', *AIAA Paper 77-716*, 1977.
17. L.K. Chang, 'The theoretical performance of high efficiency propeller', *Ph.D. Thesis*, Purdue University, 1980.
18. W.Z. Stepniewski and C.N. Keys, *Rotary Wing Aerodynamics*, Dover Publications, New York, 1984.
19. R.L. Bisplinghoff and H. Ashley, *Principles of Aeroelasticity*, Wiley, New York, 1962.
20. J. Cho, 'Frequency domain aerodynamic analyses of interaction rotating systems', *Ph.D. Thesis*, Purdue University, 1988.
21. I.H. Abbott and A.E. Von Doenhoff, *Theory of Wing Sections, Including a Summary of Airfoil Data*, Dover Publications, New York, 1959.